5-2023

Trajectory Energy Management for eCTOL: Examination of Battery Discharge Under Two Flight Profiles

Denner Campos Cunha

Trajectory Energy Management for eCTOL: Examination of Battery Discharge Under Two Flight Profiles

by
Denner Campos Cunha

A thesis submitted to the College of Engineering and Science of
Florida Institute of Technology
in partial fulfillment of the requirements
for the degree of

Master of Science
in
Flight Test Engineering

Melbourne, Florida
May, 2023

We the undersigned committee hereby approve the attached thesis,
"Trajectory Energy Management for eCTOL:
Examination of Battery Discharge Under Two Flight Profiles"
by
Denner Campos Cunha

Isaac Silver, Ph.D.
Professor
Aerospace, Physics and Space Sciences
Major Advisor

Brooke Wheeler, Ph.D.
Assistant Professor
College of Aeronautics

Ralph D. Kimberlin, Dr. -Ing.
Professor
Aerospace, Physics and Space Sciences

Razvan Rusovici, Ph.D.
Associate Professor
Aerospace, Physics and Space Sciences

David C. Fleming, Ph.D.
Associate Professor and Department Head
Aerospace, Physics and Space Sciences

Abstract

Title:
"Trajectory Energy Management for eCTOL:
Examination of Battery Discharge Under Two Flight Profiles"

Author:
Denner Campos Cunha

Major Advisor:
Isaac Silver, Ph.D.

The expanding industry of electric airplanes presents a significant regulatory challenge for aviation authorities worldwide. The first step towards achieving a precise Trajectory Energy Management (TEM) is to understand how the powertrain behaves during the operation. Therefore, this work examined the battery performance of an eCTOL, the Pipistrel Velis Electro, under two different prescribed flight profiles and take-off weights. Flight 1, a destination trip profile, was conducted with a gross weight of 1146 lbs and a constant power setting of 22 kW during the cruise segment, while Flight 2, a local training flight profile, was conducted with a gross weight of 1318 lbs and exhibited more pronounced variations in power setting. The test sorties were conducted at different outside air temperatures (OAT) and both of them were completed before SOC dropped below 40%. The analysis of motor power shows that the power generation was predictable, and the batteries' ability to supply power was consistent throughout the discharge, with a mean value of approximately 3% in power loss. However, a growing discrepancy between the state of charge (SOC) of the batteries was observed during discharge due to the difference in the state of health (SOH), resulting in one battery storing more energy than the other. The energy required analysis shows that Flight 2 had more available energy at engine start than Flight 1 due to the higher OAT during battery charging. To climb to the same altitude of 1900 ft MSL, Flight 2 required approximately 18% more energy than Flight 1. In the cruise segment, Flight 1 exhibited a specific range of 3.5 NM/kWh and specific endurance of 2.6 min/kWh with 22

kW, while Flight 2 achieved 3.9 NM/kWh and 2.9 min/kWh with 21 kW, despite the higher weight. This counterintuitive outcome is attributed to the difference in OAT and reinforces the importance of understanding the impacts of temperature on battery performance while planning the flight. Additionally, sustained turns with 30° of bank angle were performed at a target airspeed of 85 knots, requiring approximately 0.52 kWh to complete the maneuver. This represents a 17% increase in energy required compared to the amount required to trim the aircraft at a steady flight with the same airspeed. The study also highlights that the aircraft is sensitive to external factors such as airmass, air quality, and the pilot's handling techniques, where significant differences in energy required can be observed during maneuvers and flight conditions replicated in different sorties. These findings underscore the importance of considering maneuvering energy required when establishing safety margins for electric aircraft operations. This point deserves the attention of regulatory authorities, who play a critical role in ensuring safe and efficient operations.

Table of Contents

List of Figures

List of Tables

Nomenclatures

AC	Alternate Current
BMS	Battery Management System
CCCV	Constant Current Constant Voltage
CFR	Code of Federal Regulations
CG	Center of Gravity
DC	Direct Current
eCTOL	electric Conventional Take-off and Landing
EST	Eastern Standard Time
eSTOL	electric Short Take-off and Landing
eVTOL	electric Vertical Take-off and Landing
EASA	European Aviation Safety Agency
EV	Electric Vehicle
FAA	Federal Aviation Administration
FIT	Florida Institute of Technology
GA	General Aviation
GAMA	General Aviation Manufacturers Association
GPS	Global Positioning System
IFR	Instrument Flight Rules
KMLB	Melbourne Orlando International Airport
LCD	Liquid-Crystal Display
LIB	Lithium-ion Battery
Li-Ion	Lithium-ion
LSA	Light-Sport Aeroplane
LND	Landing
MAC	Mean Aerodynamic Chord
MATLAB	Matrix Laboratory
MSL	Mean Sea Level
MCP	Maximum Continuous Power
MTOP	Maximum Take-off Power
MTOW	Maximum Take-off Weight

NM	Nautical Miles
OAT	Outside Air Temperature
OCV	Open Circuit Voltage
POH	Pilot Operating Handbook
RFT	Remaining Flight Time
ROC	Rate of Climb
RPM	Revolutions Per Minute
SOC	State of Charge
SOA	Safe Operating Area
SOAP	State of Available Power
SOE	State of Energy
SOH	State of Health
TCDS	Type Certificate Data Sheet
TEM	Trajectory Energy Management
T/O	Take-off
V_h	Maximum speed in level flight with MCP
V_Y	Speed for Best Rate of Climb
VFR	Visual Flight Rules
UAM	Urban Air Mobility

Acknowledgements

I would like to express my sincere gratitude to the College of Engineering and Science of Florida Institute of Technology for providing the infrastructure to carry out this research and to the faculty for all the wisdom throughout my master's program. Also, a special thanks to my advisor and committee chair Dr. Isaac Silver for his guidance, support, and the opportunity to work on such a disruptive project. His experience as a test pilot made a significant contribution to the research as well as to my professional development.

I would also like to thank the Georgia Institute of Technology for the partnership and the Federal Aviation Administration for funding this study through the contract DTFACT-17-C-00001.

Additionally, I would like to thank Dr. Brooke Wheeler for her dedicated supervision of the Trajectory Energy Management System - Phase III.

Without God's grace, I would not have been able to go on this journey. Thank you, Lord, for all of your direction during the learning process. I also want to express my sincere thankfulness to my wife, Gabriela Cunha, for all of her love and support. Lastly, I would like to thank the Herold family for all the assistance and encouragement.

Dedication

I dedicate this to my wife, who was always there for me, especially on the toughest days.

Chapter 1

Introduction

1.1 Motivation

Electric airplanes, which are propelled by battery-powered electric motors, are one of the technological advancements now available as aviation evolves toward sustainability. Aside from being carbon-free, all-electric aircraft have the potential to substantially reduce noise pollution in airport areas.

Currently, the most common battery chemistry used in electric vehicles (EVs) is comprised of Lithium-ion (Li-Ion). This type of battery generally features a stable matrix, low internal resistance, high cycle life, and high energy density compared to other available battery technologies. However, the desired density of around 500 Wh/kg has not yet been achieved; instead, 150 to 250 Wh/kg is more often available [16]. To put it into perspective, Avgas or Jet-A can hold around 50 times more energy per unit mass than conventional Li-Ion batteries [15]. As a result, researchers are studying new technologies to enhance existing airplane battery alternatives.

As aviation moves to electrify aircraft, the Federal Aviation Administration (FAA), and regulators worldwide, face a significant challenge in adjusting/replacing existing regulations to accommodate this expanding industry. In recent years, hundreds of companies, ranging from large aircraft manufacturers to new start-ups, have been designing and prototyping electric vehicles with vertical take-off and landing capabilities, the so-called eVTOLs. These vehicles, known as Urban Air Mobility (UAM) vehicles, are conceived for personal transportation in predominantly metropolitan and inter-metropolitan areas. Because of their unique design concepts, such as reduced energy storage capacity and the dynamic nature of the powertrain system, the FAA announced that eVTOLs will be certified as a special class of powered-lift aircraft under Part 21.17(b), instead of traditional aircraft under Part 23 of title 14 of the Code of Federal Regulations (14 CFR 23) with special conditions [2].

Existing FAA standards for civil aviation are only applicable to fuel-burning aircraft. One of the obstacles when using 14 CFR 23 for eVTOL vehicle certification is the issue of energy margins and the associated trajectory power and energy management [4]. It must always be ensured that the vehicle has enough energy stored in its batteries to safely accomplish a mission with adequate margins, and the information concerning power and energy requirements as well as availability must be continually sent to a pilot or a control system. If the estimated power required to maintain a flight condition or the energy required to safely accomplish a maneuver exceeds the available reserves, the pilot must be alerted and provided with a proposed plan of action [18].

When it comes to electric propulsion, one of the key regulatory and technical challenges is related to energy reserve. Traditional aircraft must communicate to the operator the instantaneous power available and the remaining energy reserves, which is a primary driver of cockpit instrumentation requirements. Accordingly, the minimum fuel requirements are specified by 14 CFR 91.

For fixed-wing aircraft under Visual Flight Rules (VFR), 14 CFR §91.151 states that no person may begin a flight unless there is enough fuel onboard to reach the first point of intended landing and to fly at normal cruise speed for at least 30 minutes (during the day) or 45 minutes (at night) afterward. For rotorcraft under VFR, sufficient fuel for at least another 20 minutes of flight at normal cruise speed is required after reaching the intended destination.

In addition, 14 CFR §91.167 states the fuel reserve for a flight under Instrument Flight Rules (IFR). The airplane must have fuel onboard to continue flying for a further 45 minutes at cruise speed after reaching the first intended destination. For rotorcraft, 30 minutes of fuel reserve is required. Most probably, current electric-powered aircraft are unlikely to meet those requirements and, therefore, alternative means of compliance should be designed for those vehicles.

The energy reserve for any aircraft shall be determined to ensure safe flight operation, including reaching a possible alternate area to provide the aircrew with time to complete the flight [18]. This endurance calculation is a well-known procedure for traditional fuel-burning aircraft and it is based on the amount of fuel remaining in the tanks. Furthermore, the aircraft gets lighter as fuel is burned, allowing it some extra power at the end of the mission. Indeed, Advisory Circular 23-17C remarks that the primary instrument for fuel remaining shall be the fuel quantity indicators in the instrument panels. However, for an electric powertrain, the gross weight of the vehicle in flight does not decrease but remains constant. In that sense, the ability to define overall energy available and energy consumption depends on understanding the new metrics that may be required to characterize the energy state [17].

One of the most important ways to avoid fuel exhaustion is to ensure that pilots are aware of the aircraft's trajectory energy state at all times. That implies that pilots must understand how much energy is required to safely complete a flight mission, how much power is required to complete a certain phase, and how much fuel reserve the aircraft holds. Even though engine efficiency and fuel density can change depending on temperature, the amount of energy stored in a certain volume of kerosene is always predictable and well-defined. On the other hand, energy and power accessed from batteries depend on their cycle life, temperature, cutoff voltage, and charge/discharge rate, among other factors. Essentially, it is difficult to calculate the remaining energy level without taking into account the battery's current state, current environment, and operational and environmental history. Those peculiarities of electric propulsion combined with vertical take-off and landing capability – where the aircraft is unable to glide or autorotate to perform a safe emergency landing – necessitate a precise Trajectory Energy Management (TEM) to ensure safe operation. Thus, the TEM task entails the manipulation of flight and propulsion controls to accomplish a prescribed flight profile [18].

According to [18], in order to gain a detailed picture of the characteristics of electric powertrains and operational requirements, regulators may require manufacturers to use onboard computers that run predictive trajectory power and energy models, along with tests based on conservative methods. Thereby, the purpose of TEM Systems is to close the feedback loop to the operators so that they are aware of the aircraft's observed and predicted power and energy states.

1.2 Objectives

Regulators are still unfamiliar with electrical propulsion, even for general aviation Conventional or Short Take-off and Landing aircraft (eCTOL/eSTOL). The European Aviation Safety Agency (EASA) currently has one model commercially certified, the Pipistrel Velis Electro. The Light-Sport Aeroplane (LSA), however, is not certified in the United States, where it operates as an experimental aircraft. According to European authority standards, a minimum flight time reserve of 10 minutes in battery charge is required for operations at an airport under EASA regulations [3].

The primary objective of this study is to examine the flight data collected from the Velis Electro, a full-scale electric conventional takeoff and landing (eCTOL) aircraft, during two test sorties with distinct take-off weights and prescribed flight profiles, namely a Destination Trip and a Local Training Flight. The study aims to analyze the flight data obtained from the aircraft, with a focus on key parameters such as state of charge, available energy, remaining flight time, battery temperature, motor power, motor RPM, torque, voltage, current, and battery internal resistance, starting from a

full (100%) charge. All the data collection will assist the FAA in establishing means of compliance regarding energy and power requirements for certification of the upcoming generation of electric-powered aircraft.

1.3 Test Article

The Pipistrel Velis Electro, manufactured by Pipistrel Vertical Solutions d.o.o. in Ajdovščina - Slovenia [13], is the world's first electric-powered airplane to receive a Type Certificate from EASA in June 2020 (EASA.A.573 TCDS) for VFR operations; but the LSA operates under the experimental category in the United States. The aircraft has an endurance of roughly one hour. However, due to 14 CFR § 91.151, the pilot must prepare to land with 30 minutes of estimated remaining flight time. The experimental aircraft used for testing has registration code N880HM and serial number VSWX1280032 (Figure 1.1).

The Velis Electro is a two-place, high-wing, T-tail design, powered by a single motor. It was designed based on its pre-certified variant, Pipistrel Virus SW, which is powered by a four-cylinder piston engine that produces 80 hp at 5800 RPM. Rather than a reciprocating engine, the Velis Electro is powered by an electric axial-flux motor designed to produce a MTOP of 57.6 kW at 2500 RPM for 90 seconds. Mounted to the motor shaft, a 3-blade ground adjustable propeller of 65 in diameter generates thrust. The motor is supplied by two 11kWh lithium-ion battery (LIB) packs (featuring manganese, nickel, and cobalt chemistry), which are located fore and aft of the cabin. In an eventual battery failure, the faulty battery gets automatically disconnected from the system. The batteries are controlled by the Battery Management System (BMS), which continually monitors and manages battery parameters during charge and discharge. The aircraft's power electronics system is a power controller/inverter, which is supplied by direct current (DC) from the batteries and provides a 3-phase alternating current (AC) to the motor in a maximum continuous current of 300 A.

The Velis has a wingspan of 35.13 ft, a mean aerodynamic chord of 2.94 ft, and a total wing area of 102.36 ft^2. Its maximum takeoff weight (MTOW) is 1323 lbs, considering a design empty weight of 926 lbs and a maximum payload of 380 lbs. At this weight and at sea level flight, the aircraft presents a cruise speed of 69 kts at minimum power for level flight (20 kW) and 93 kts at maximum continuous RPM power (36 kW) [13].

Figure 1.1: Test Aircraft Pipistrel Velis Electro, N880HM.

Figure 1.2 shows the aircraft's electric propulsion system components and Tables 1.1 and 1.3 summarize technical information about them, according to [13].

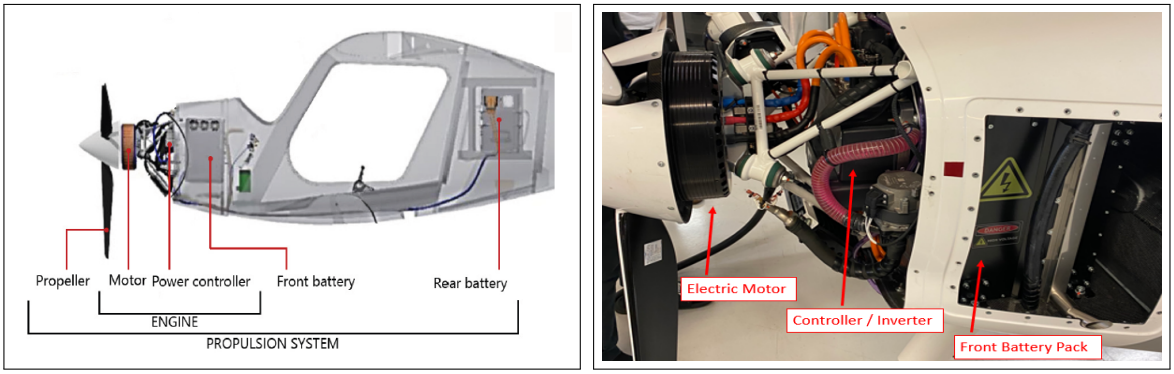

Figure 1.2: Electric Propulsion System Components in Velis Electro [13].

Table 1.1: Technical Information About the Electric Motor [13].

Electric Motor (axial-flux 3-phase AC)	Pipistrel electric engine E-811-268MVLC
Maximum take-off power (MTOP)	57.6 kW (limited to 90 sec)
Maximum continuous power (MCP)	49.2 kW
Maximum take-off RPM	2500 RPM (electronically limited)
Maximum continuous RPM	2350 RPM
Motor temperature	min -20°C, max +110°C

Table 1.3: Technical Information About the Battery Packs and Power Controller [13].

Li-Ion Battery Pack	Pipistrel PB345V124E-L batteries
Mass	158.73 lb
Maximum continuous discharge power	40 kW
Maximum discharge current	120 A
Maximum voltage	394 V
Minimum voltage	260 V
Operating temperature range (discharge)	0°C - 58°C
Operating temperature range (charge)	0°C - 45°C
Rated capacity (@23°C, 20 A discharge current)	33 Ah, 11 kWh
Minimum Performance Take-off Power (MPTOP)	50 kW (low battery SOH)
Power Controller	H300C power-electronics
Operating temperature	min -20 °C, max +70°C

To keep the temperature within the operating limits, the electric motor, battery packs, and power controller are liquid-cooled. The system relies on radiators and electrically driven pumps, with a solution of 50% distilled water and 50% glycol automotive grade G12+ as coolant. The air inlet for the radiator is placed on the left side of the fuselage, whereas the hot air is exhausted from the bottom, through an exhaust outlet (Figure 1.3). For ground operations, such as battery charging, small fans installed behind the radiator and controlled by the BMS are responsible for the battery cooling.

Figure 1.3: Velis Electro Powertrain Cooling System.

1.4 Test Area and Test Conditions

Flight testing with experimental aircraft tail number N880HM occurred at Melbourne Orlando International Airport (KMLB), located in Melbourne, Florida. Both of the flight sorties were conducted to the Southeast of the airfield, as detailed in Section 3.2. Figure 1.4 highlights the play area, within the red polygon, which FIT test pilots commonly use during the execution of flight test laboratories.

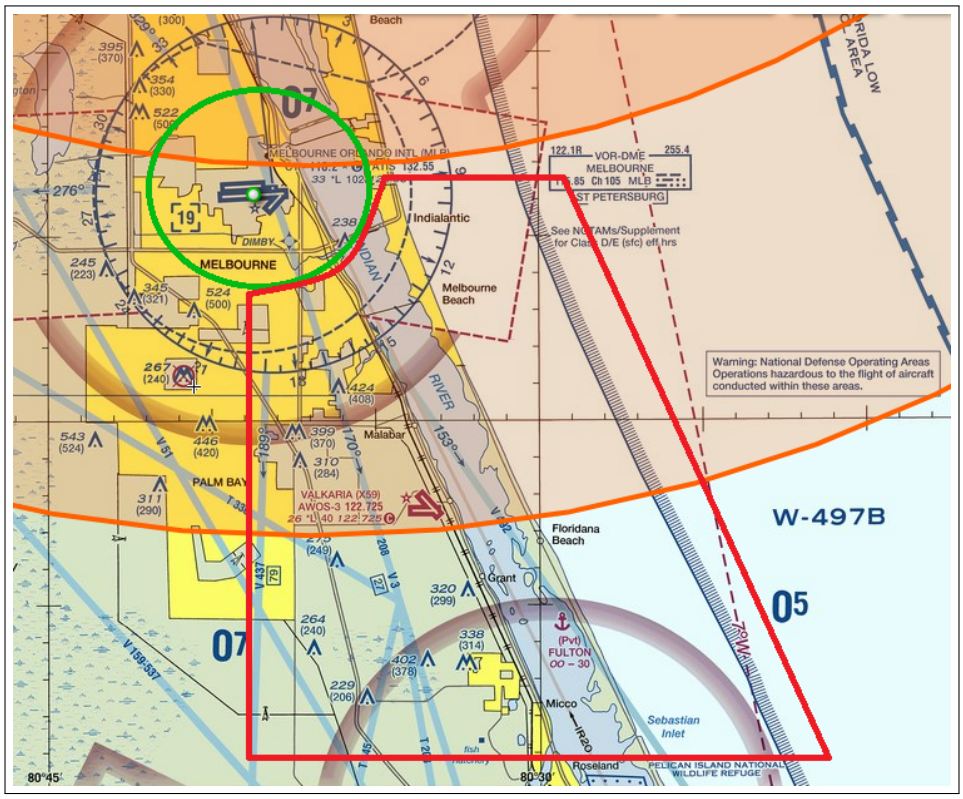

Figure 1.4: Flight Test Area Used by FIT (Red Polygon).

The sorties were performed on 02/16/2023 (Flight 1), between 07:00 and 07:40 AM, and 03/17/2023 (Flight 2), between 7:30 and 8:05 AM. The flights were completed in a calm atmosphere, without any unforeseen weather occurrences, and with visual conditions. The meteorological conditions at the time of testing are summarized in Table 1.5.

Table 1.5: Meteorological Information at KMLB During Testing.

Flight	Wind Speed	Visibility	Condition	OAT	Pressure
1 (T/O)	0 kts	10 sm	Fair	11 °C	30.07 inHg
1 (LND)	0 kts	10 sm	Fair	14 °C	30.09 inHg
2 (T/O)	0 kts	10 sm	Fair	15 °C	30.05 inHg
2 (LND)	0 kts	10 sm	Fair	17 °C	30.04 inHg

Chapter 2

Background

To understand how a battery operates in different conditions, it is important to know how the cell characteristics depend on the battery status [5]. Since electric propulsion technology is handled differently than current propulsion systems, distinct powertrain key metrics need to be considered such as State of Charge (SOC), State of Health (SOH), State of Energy (SOE), State of Available Power (SOAP), and voltage/temperature effects.

2.1 State of Charge (SOC) & State of Health (SOH)

The SOC is a popular metric for estimating how much electrical energy remains in a battery. According to [19], the estimation of SOC is meant to achieve two goals in terms of battery performance. To begin, SOC indicates the amount of energy a battery has remaining when compared to the amount of energy it had when fully charged. Second, the metric provides the operator with an estimation of how long a battery will last before the need to be recharged. The accuracy of SOC estimation is of crucial importance to the operational safety of a battery pack [19]. Thus, SOC is an established metric for assessing the energy remaining in a battery, which provides a dimensionless ratio between the available charge at any given time and the total battery capacity [14]. The SOC varies between 0% (completely discharged) and 100% (fully charged).

It is important to highlight that the maximum charge that a battery can hold is related to its present SOH value, which is the ratio between releasable capacity and rated capacity [10], i.e. the nominal maximum charge when its cells were new. Battery degradation and decrease in SOH are driven by a number of factors, most notably the age of the battery, the cycle life, and the charge and discharge temperatures. Battery aging is the gradual decrease in discharge capacity caused by the increase of internal resistance [18]. This means that for an aged cell, a 100% SOC can be equivalent to a 75%–80% SOC of a new cell.

Unlike a fuel quantity, SOH and SOC cannot be easily measured or calculated directly from electrical parameters but can be estimated from other measurements [18]. In theory, battery cell voltage is an indication of SOC, but only within a linear range of around 80% to 20% of battery charge, as shown in Figure 2.1.

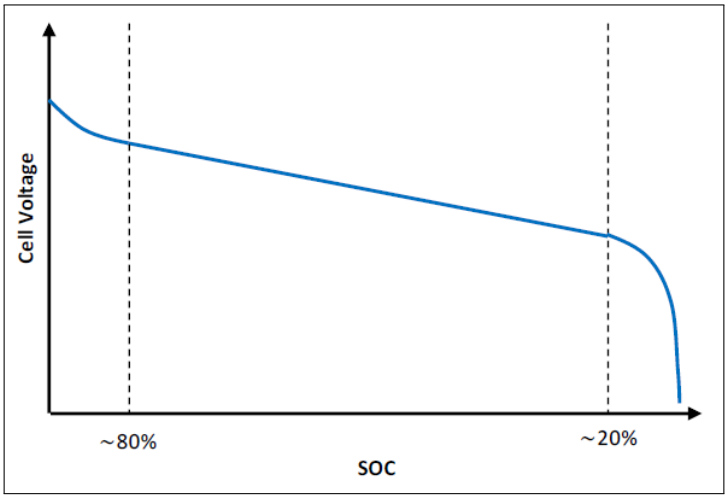

Figure 2.1: Typical Cell Voltage vs. Discharge Curve of a Generic Battery [18].

2.2 State of Energy (SOE)

The SOE reflects the amount of energy that can be extracted from the battery at a given time. This metric, which does not have a standard methodology for estimating it, is not simply the product of SOC and SOH, as it is highly dependent on the discharge rate (i.e. power required by the motor controller) and the temperatures of the individual components [18]. Since SOE encompasses the performance of the complete powertrain system, it cannot be estimated only using the available battery parameters [18].

In this study, the "available energy" is used as a parameter to characterize the amount of kWh that the battery cells can supply to the motor at a specifically commanded power setting. The available energy differs from the storage energy since it accounts for energy losses due to thermal effects.

LIBs, like all other battery chemistries, have a capacity increase with increasing cell temperature [11] and a capacity decrease as they age [12] (see Figures 2.2 and 2.3).

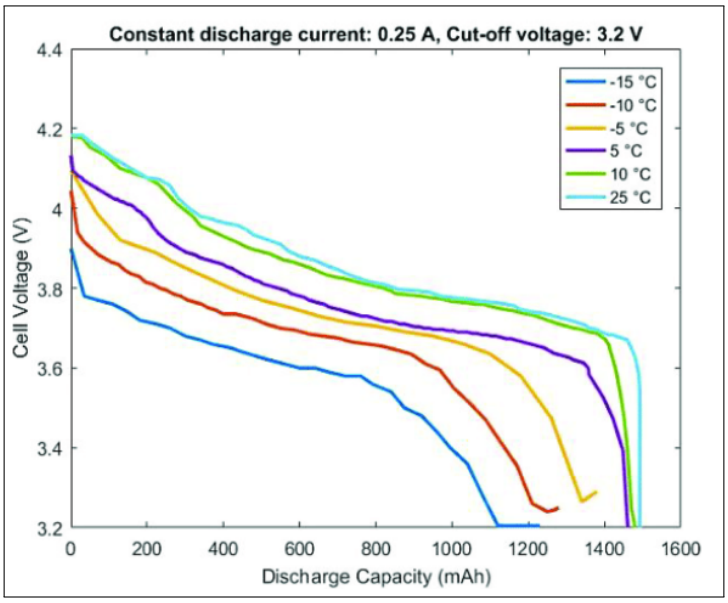

Figure 2.2: Cell Voltage vs. Discharge Capacity at Various Temperatures [11].

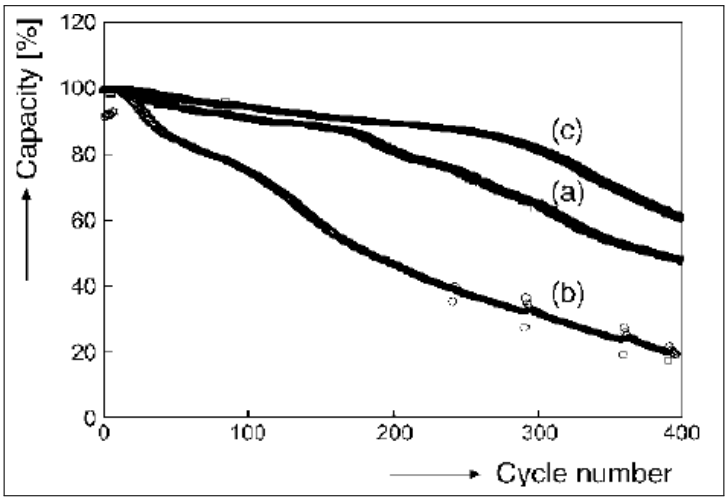

Figure 2.3: Cycle Life of Cylindrical LIBs Under High Charging Load Conditions at (a) I_{max} = 4.5 C, V_{max} = 4.2 V (b) and I_{max} = 4.5 C, V_{max} = 4.3 V, and (c) I_{max} = 1 C, V_{max} = 4.2 V (Cycle Life Upon Standard CCCV-Charging) [12].

2.3 State of Available Power (SOAP)

The SOAP indicates the maximum power that can be drawn from the battery [18]. The available battery power is determined by the Safe Operating Area (SOA), which is limited by battery temperature, discharge current, battery voltage, and SOC [1]. Therefore, the maximum extractable power is limited by the voltage and current limits

of the battery, where the limits of individual cells can be the driver [1].

Figure 2.4 presents the available power dependency on the temperature in a generic battery. It should be noted that as the temperature decreases, so does the available power. This effect is a consequence of the increase in battery internal resistance, which generates a higher voltage drop. Typically, batteries deliver their best power output when they operate at a certain optimal temperature range [5].

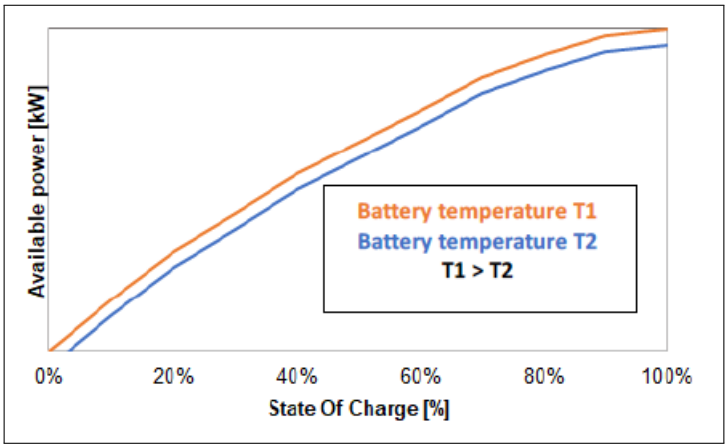

Figure 2.4: Battery Temperature Effect in Available Power Along the Discharge Curve [5].

The internal resistance of a battery is also affected by aging. As the battery ages, its internal resistance increases, causing a continuous deterioration in the maximum power that the battery can deliver [5]. Figure 2.5 compares available power at different battery SOH levels, where the aging effect can be observed.

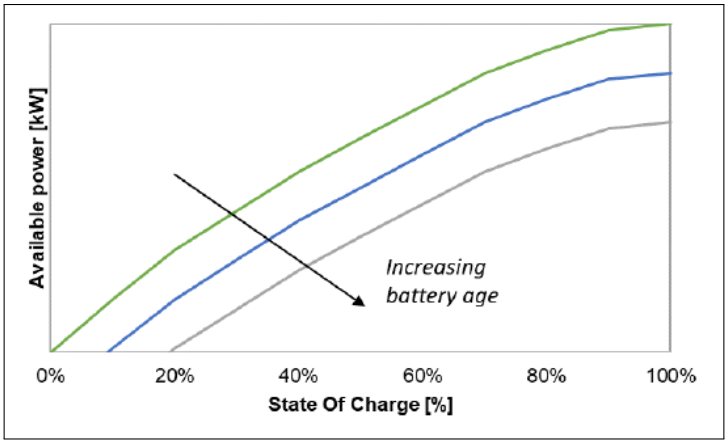

Figure 2.5: Battery Aging Effect in Available Power Along the Discharge Curve [5].

The available power is maximum in the SOC top range and gradually drops with decreasing SOC, eventually reaching 0 kW for an empty battery, as depicted in Figure 2.6. Depending on the battery specifications, the available power may feature an optimal value between 80%-90% SOC, with a slight drop around 100%, and a degradation for low SOC ranges [5]. The power degradation depends on the battery type and configuration, and some may be more severe than others.

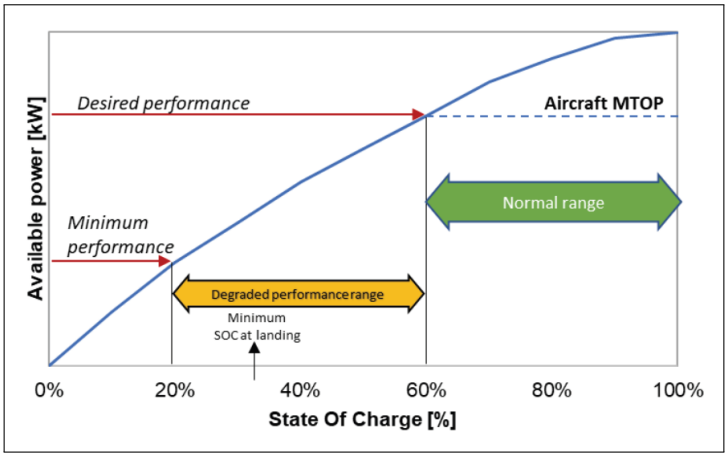

Figure 2.6: Available Power vs. SOC% Curve of a Generic Battery [5].

Finally, as more power is used during the discharge cycle, less energy is available for the propulsion system and, naturally, the faster the discharge [5]. Figure 2.7 below shows a series of graphs relating the available energy for propulsion to the percentage of maximum power used, considering also the effects of aging and temperature, as previously discussed. In this sense, it is of paramount importance that operators are aware of power management – in order to safely plan and execute a flight mission – and power degradation and its impacts on aircraft performance.

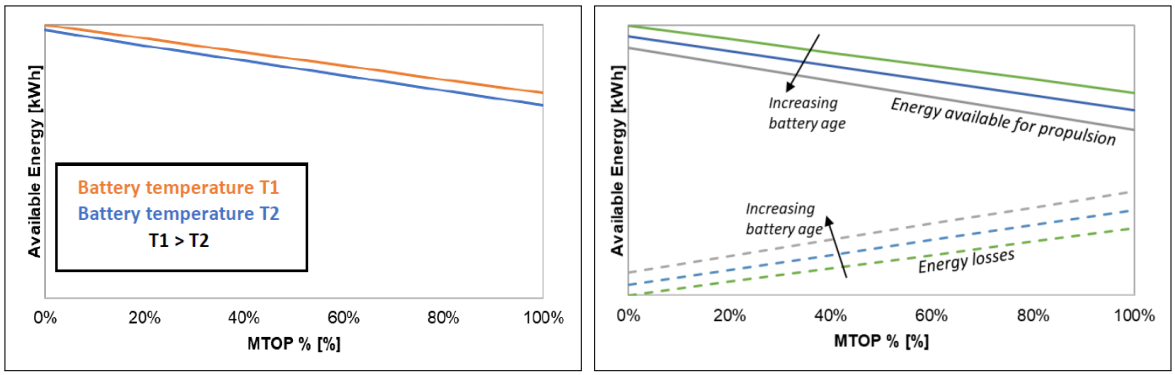

(a) Considering Temperature Effect.

(b) Considering SOH Effect.

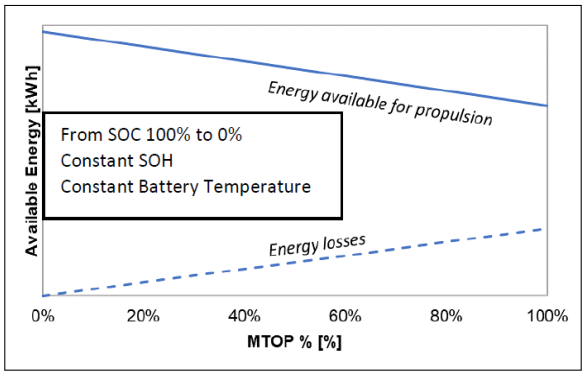

(c) Neglecting the Effects of SOH and Battery Temperature.

Figure 2.7: Available Energy vs. Power Setting as a Percentage of MTOP [5].

Chapter 3

Methodology

3.1 Instrumentation

Velis Electro is equipped with a single communication radio, transponder, and a combination of analog and digital gauges (see Figure 3.1). In operation, the system controller collects data from the power controller, motor, battery packs, and other electrical systems. The data is presented on a LCD located on the right-hand side of the cockpit, the Pipistrel's electric propulsion system instrument display, as presented in Figure 3.2. The BMS constantly calculates and reports at a rate of 5 Hz the batteries' SOC, SOH, voltage, current, temperature, etc. On the top, the aircraft features a VFR GPS display for navigation.

On the left-hand side of the instrument panel, an integrated attitude and air data display serve as the primary flight instrument. Next to it, there is an analog airspeed indicator and altimeter. Located below is the power and RPM instrumentation for the motor, as well as an inclinometer and a vertical speed indicator.

The aircraft is also equipped with a robust data logger, which can be assimilated into a flight data recorder and accessed in an Excel file as a final result. All instrumentation and battery management data channels are recorded at alternating frequency intervals of 5 and 10 Hz. This recorded data served as the primary source for data analysis.

Figure 3.1: Velis Electro N880HM Instrument Panel.

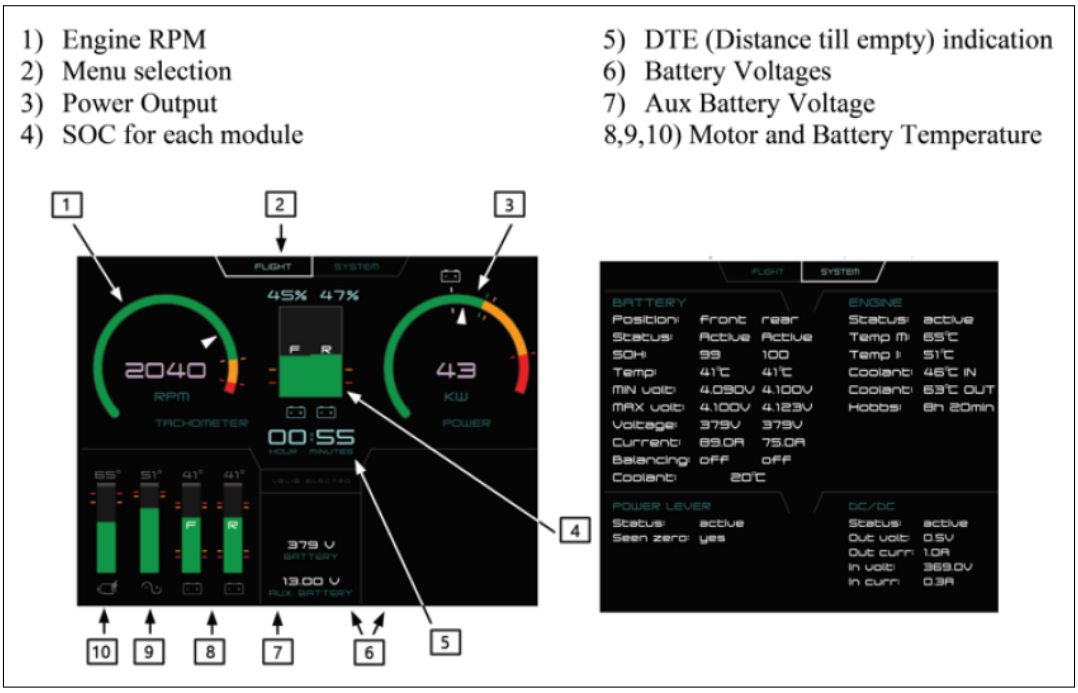

Figure 3.2: Pipistrel's Electric Propulsion System Instrument Display [13].

3.2 Reference Flight Profiles

Flight tests should be based on operationally relevant trajectories, involve realistic operating conditions, and be repeatable to offer convincing results. In order to adhere to this principle, two reference flight profiles were created based on operational scenarios proposed by the General Aviation Manufacturers Association (GAMA) [6].

The GAMA is a global trade association representing over 90 of the world's leading manufacturers of general aviation airplanes and rotorcraft, engines, avionics, components, and related services [6]. Publication 16, Hybrid & Electric Propulsion Performance Measurement, is frequently used as a baseline in hybrid and electric aircraft research. The publication includes four reference scenario-based missions, presented in Figure 3.3, to facilitate a common understanding of how to categorize and measure the performance of these aircraft: Destination Trip (A to B Transportation), Local Training Flight (A to A Flight), Traffic Pattern Flight, and Vertical Flight (A to B).

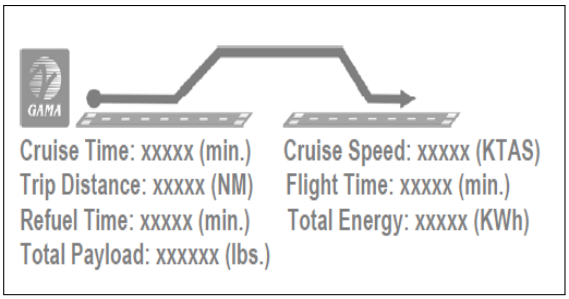

(a) Destination Trip (A to B).

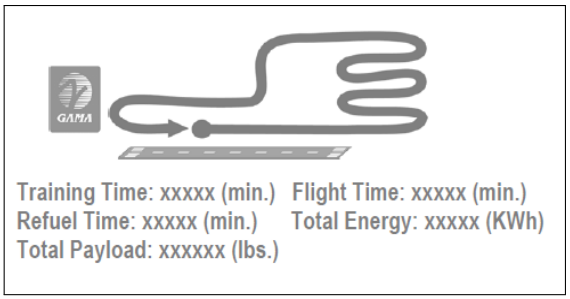

(b) Local Training Flight (A to A Flight).

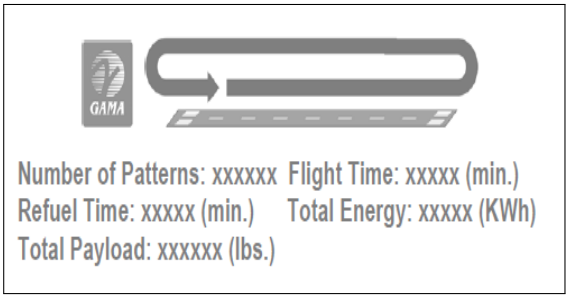

(c) Traffic Pattern Flight.

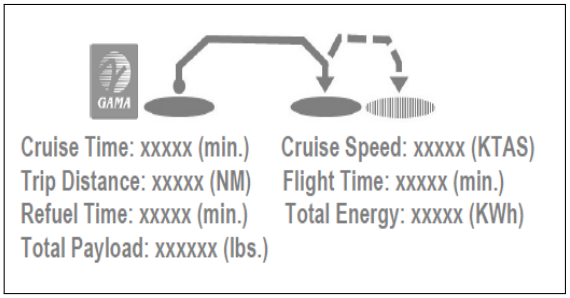

(d) Vertical Flight (A to B).

Figure 3.3: Reference Scenario-Based Missions Proposed by GAMA [6].

To represent the main mission types commonly flown by General Aviation (GA) aircraft, the team selected two GAMA profiles: a destination trip mission from point A to point B (Flight 1), and a local training flight involving a local flight from point A to point A (Flight 2).

3.2.1 Flight 1: Destination Trip Test Profile

The test card was developed utilizing the performance specifications of the aircraft, as provided in the POH. The document presents tables with the expected endurance for local flights and endurance/range for cross-country flights (A-B), ensuring 30 minutes of energy reserve at 20 kW. However, due to the limited endurance of the Velis Electro, Flight 1 had to be modified to a destination trip from point A to point A, which is still representative of the transportation mission type commonly flown by GA aircraft. The test sortie should be conducted at a minimum consumption continuous power setting, simulating a maximum-range type flight. Table 3.1 presents the mission segments for Flight 1.

Table 3.1: Flight 1: Mission Segments.

Section	**Event**	**Description**
1	Taxi	Taxi to the runway.
2	Take-off	Normal take-off procedure.
3	Climb	V_Y to 2000 ft MSL.
4	Cruise	a) Cruise at 22 kW power setting for 10 min. b) Perform a 180° turn at constant airspeed and altitude. c) Maintain a power setting of 22 kW during cruise until reaching the glide slope.
5	Landing	Begin descending, fly conventional base and turn final, and land.
6	Taxi	Normal taxi procedures.
7	Reserve	30 minutes reserve at cruise power remaining at end of flight.

3.2.2 Flight 2: Local Training Test Profile

As a training flight profile, this flight incorporates sustained turns with 30° of bank angle and simulated power-off descents at a constant airspeed. Consequently, the flight is anticipated to exhibit more pronounced variations in power setting and load factor in comparison to Flight 1. Table 3.3 presents the mission segments for Flight 2.

Table 3.3: Flight 2: Mission Segments.

Section	Event	Description
1	Taxi	Taxi to the runway.
2	Take-off	Normal take-off procedure.
3	Initial Climb	V_Y to 2500 ft MSL.
4	Training Maneuvers	a) Execute 360° level turn. b) Cut power, descend 500 ft while maintaining 65 kt. c) Execute 360° level turn. d) Climb 500 ft. e) Cut power, descend 500 ft while maintaining 75 kt. f) Climb to 500 ft. g) Cut power, descend 500 ft while maintaining 85 kt. h) Trim the aircraft at different power settings.
5	Landing	Begin descending, fly conventional base and turn final, and land.
6	Taxi	Normal taxi procedures.
7	Reserve	30 minutes reserve at cruise power (based on speed & altitude used for training above) remaining at end of flight.

3.3 Test Procedure

Two test flights were conducted – Flight 1 and Flight 2 – with different weight configurations and based on different flight profiles, as detailed in Section 3.2. The battery packs were charged via on-board charging port, and a complete charging procedure (100% SOC) at a current of 50 A was carried out before each flight (Figure 3.4).

Figure 3.4: Charger Display After Full Charge Procedure.

The charging method utilized in the Velis Electro aircraft is based on the Constant Current Constant Voltage (CCCV) charging protocol, which is of crucial importance to ensure optimal performance and safety of the batteries. This protocol is a typical method of charging rechargeable batteries and consists of two stages [5]. The first stage starts with a constant current that is applied to the battery until the voltage reaches the target level. During the second stage, the current is reduced regularly to maintain the target voltage level until the battery is fully charged. The charging process ends when the current reaches 0 A and the voltage reaches the Open Circuit Voltage (OCV) for SOC 100%. The CCCV charging protocol is designed to prevent overcharging of the batteries, which can lead to safety hazards such as thermal runaway and fire. Additionally, this protocol helps to prolong the lifespan of the batteries by minimizing their stress over the charging process.

Figure 3.5 shows time series charts of the batteries recharging prior to Flight 2, where compliance with the CCCV protocol is observed. Furthermore, it is noteworthy that the BMS effectively maintains the average temperature of the battery cells at 22°C. The charging temperature inside the hangar was 19°C.

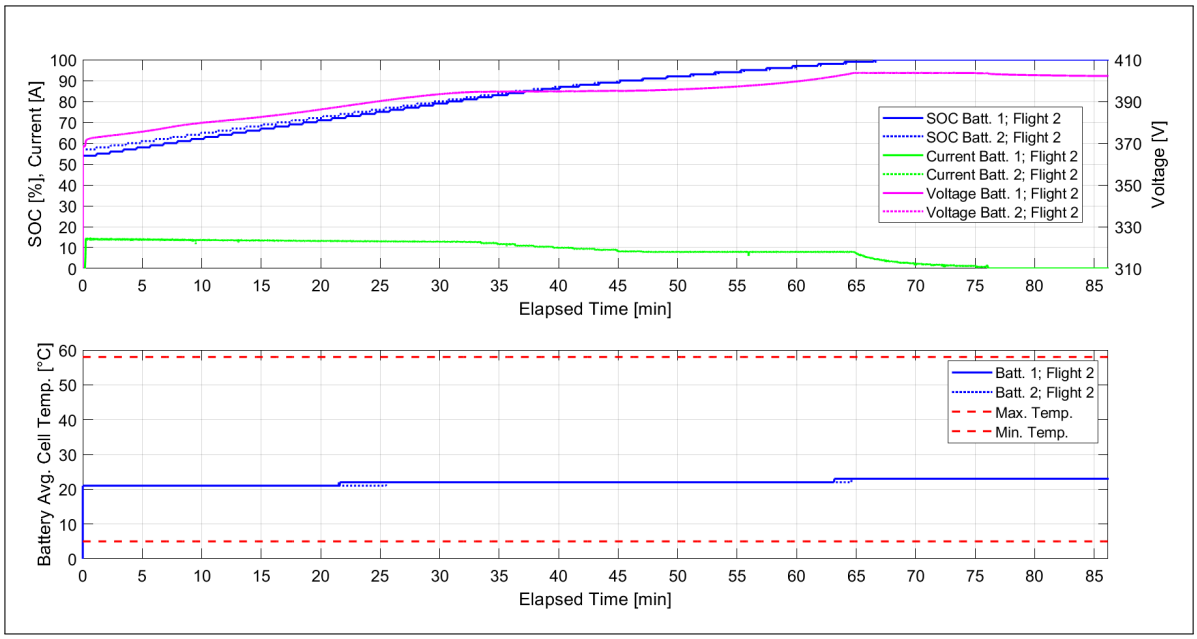

Figure 3.5: Battery Packs Recharging Prior to Flight 2.

The Velis Electro differs from conventional airplanes in that it does not undergo weight changes during flight since it does not burn fuel. Moreover, it does not have a baggage compartment, so the gross weight and CG are influenced only by the crew. Tables 3.5 and 3.7 present the Weight & Balance calculation for both flights and Figure 3.6 depicts the aircraft's CG envelope. The envelope restrictions are given in percent of mean aerodynamic chord by the POH [13]. These values were converted to inches from the given datum of the leading edge at the wing root. As shown in Figure 3.6, the weight and CG of N880HM were within the acceptable limits in both flights.

Equation 3.1 was used to calculate the CG position expressed as %MAC.

$$CG_{\%MAC} = 100 \times \frac{CG_{in} - 1.693}{35.315} \tag{3.1}$$

Table 3.5: Flight 1: Weight & Balance Calculation.

	Weight [lbs]	Arm [in]	Moment [in.lbs]
Aircraft Empty Weight	926	10.6	9814.5
Pilot	220	14.6	3212
Co-pilot	0	14.6	0
Total Weight / Moment	1146	-	13026.5
Center of Gravity	-	11.4	-

Table 3.7: Flight 2: Weight & Balance Calculation for Flight 2.

	Weight [lbs]	Arm [in]	Moment [in.lbs]
Aircraft Empty Weight	926	10.6	9814.5
Pilot	220	14.6	3212
Co-pilot	172	14.6	2511.2
Total Weight / Moment	1318	-	15537.7
Center of Gravity	-	11.8	-

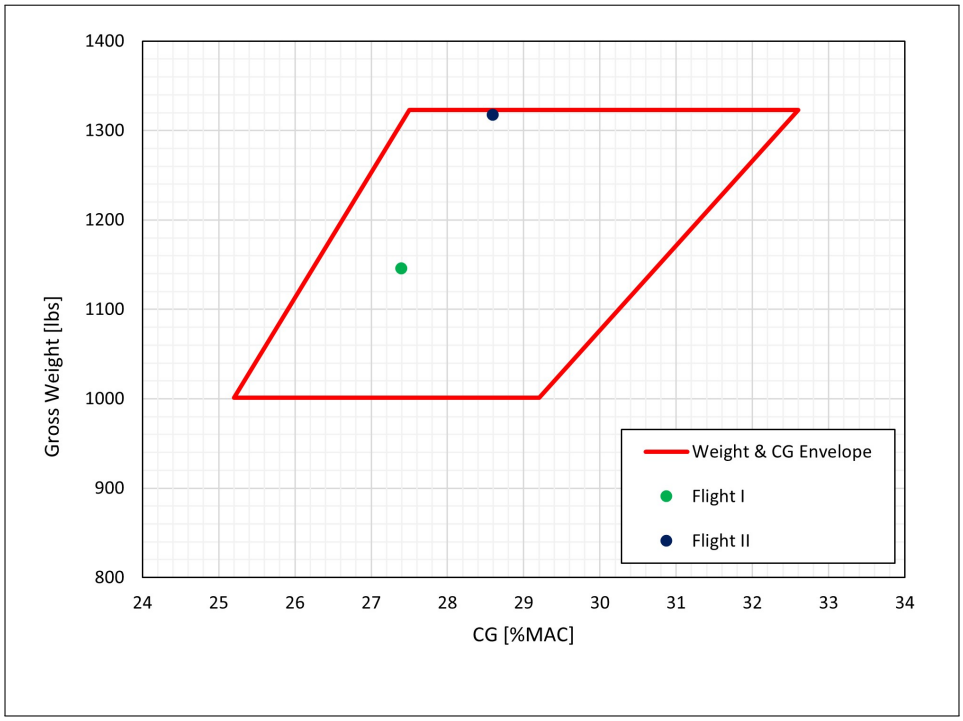

Figure 3.6: Velis Electro Weight and CG Envelope.

3.4 Data Reduction

The parameters collected by the data logger were processed online by a Pipistrel browser-based tool and made available in Excel files. Subsequently, the applicable parameters (summarized in Table 3.9) were handled in MATLAB. Both position and instrument errors in airspeed and altitude are assumed to be equal to zero.

Table 3.9: Parameters Provided by the Flight Data Recorder Used for the Data Analysis.

Parameter	**Unit**
Average Cells Temp. (Battery Packs 1 & 2)	°C
Available Energy (Battery Packs 1 & 2)	kWh
Current (Battery Packs 1 & 2)	A
Elapsed Time	sec
Indicated Airspeed	kt
Latitude & Longitude	degrees
Motor Power	kW
Motor RPM	rpm
Motor Temperature	°C
Normal Load Factor	-
Outside Air Temperature	°C
Pressure Altitude	ft
Remaining Flight Time	min
Requested Torque	% max. torque
SOC (Battery Packs 1 & 2)	%
SOH (Battery Packs 1 & 2)	%
Voltage (Battery Packs 1 & 2)	V

Additionally, other parameters were calculated from the data output. In physics, power is the measure of the rate at which work is done or the rate at which energy is transferred. Its magnitude can be calculated according to the equation below:

$$P = F \times v \tag{3.2}$$

P : Power [W]
F : Force Acting in the Particle [N]
v : Instantaneous Velocity [m/s]

Since electric motors involve a rotating shaft, as in a reciprocating engine, power can

be related to the rotational properties of torque and angular speed (equation 3.3).

$$P_{Motor} = Q_{Motor} \times RPM \times \frac{2\pi}{60} \tag{3.3}$$

P_{Motor} : Motor Power [W]
Q_{Motor} : Motor Torque Output [N.m]
RPM : Motor Revolutions per Minute [rpm]

Electric power is the rate at which electrical energy is transferred by an electric circuit. For a resistor in a DC circuit, the power is calculated by the following equation:

$$P_{Bat} = V_{Bat} \times I_{Sys} \tag{3.4}$$

P_{Bat} : Battery Power Available [W]
V_{Bat} : Battery Voltage [V]
I_{Sys} : Electric Current In the System [A]

Finally, battery internal resistance can be calculated using Ohm's Law (equation 3.5).

$$R_{Bat} = \frac{V_{Bat}}{I_{Sys}} \tag{3.5}$$

R_{Bat} : Battery Internal Resistance [Ω]

"The airplane's ability to cover great distances by conversion of fuel energy into airspeed and its ability to use this same energy to stay aloft over a period of time are performance parameters of great importance [8]". The determination of specific range (SR) and specific endurance (SE) is a convenient method of expressing an airplane's range or endurance. The SR can be defined as the ratio between nautical miles traveled and pounds of fuel consumed. SE, on the other hand, can be defined as the ratio between hours flown and pounds of fuel consumed. The Breguet equations are a well-established means of estimating the range and endurance of piston and jet engine aircraft. However, when it comes to electric aircraft, such estimates are not well established and may not follow the typical format used in the aeronautics community [9]. In order to bring this concept to an electric aircraft scenario, where Breguet equations are no longer applicable, and compare the range/endurance between both test sorties, the following equations were used:

$$SR = \frac{Nautical\,Miles\,Traveled}{Energy\,Required} \tag{3.6}$$

$$SE = \frac{Minutes\,Flown}{Energy\,Required} \tag{3.7}$$

SR : Specific Range [NM/kWh]
SE : Specific Endurance [min/kWh]

It is important to bear in mind that range and endurance may vary from flight to flight due to the Peukert Effect, which describes the impact of current draw on the battery's behavior and effective capacity. This effect is dependent on several factors, including battery type, temperature, and age [9].

The steady climb is one of the techniques used in performance testing to determine the climb performance [8]. This method is used generally for low-speed aircraft and the vector approach can be applied if we assume: 1) a small angle of attack, 2) a thrust line acting along the direction of flight, and 3) that the aircraft is climbing and accelerating in the direction of flight. Applying Newton's second law, the observed rate of climb (ROC_{OBS}) can be expressed according to the following equation:

$$ROC_{OBS} = \frac{dH}{dt} \tag{3.8}$$

To correct ROC_{OBS} for nonstandard temperature equation 3.9 is used.

$$ROC_{TC} = ROC_{OBS} \times \frac{OAT + 273.15}{T_S + 273.15} \tag{3.9}$$

ROC_{TC} : Observed ROC Corrected Nonstandard Temperature [ft/min]
T_S : Standard Day Temperature [°C] (=15°C)

Chapter 4

Results

The main objective of the tests was met. Two test sorties, Flight 1 and 2, under different weight configurations were performed based on the test profiles introduced in Section 3.2. Table 4.1 states basic information about the flights and Figure 4.1 shows the specific flight paths of the N880HM over the test area. In order to comply with the 14 CFR § 91.151, each flight was endurance limited and lasted under 30 minutes from take-off to landing.

Table 4.1: N880HM General Test Testing Info.

	Flight 1	Fight 2
Date	02/16/23	03/17/23
Engine Start Time (EST)	07:11 AM	7:36 AM
Engine Shutdown Time (EST)	07:47 AM	8:05 AM
Gross Weight [lb]	1146	1318
Duration [min]	36	29
Battery	Pack 1 / Pack 2	Pack 1 / Pack 2
SOH [%]	92 / 99	88 / 99
Initial SOC [%]	100 / 100	100 / 100
Final SOC [%]	42 / 45	47 / 51
Initial Avail. Energy [kWh]	10.10 / 10.15	9.85 / 10.27
Final Avail. Energy [kWh]	4.02 / 4.31	4.56 / 5.01
Initial Avg. Cells Temp. [°C]	15 / 15	20 /19
Final Avg. Cells Temp. [°C]	18 / 18	22 / 22

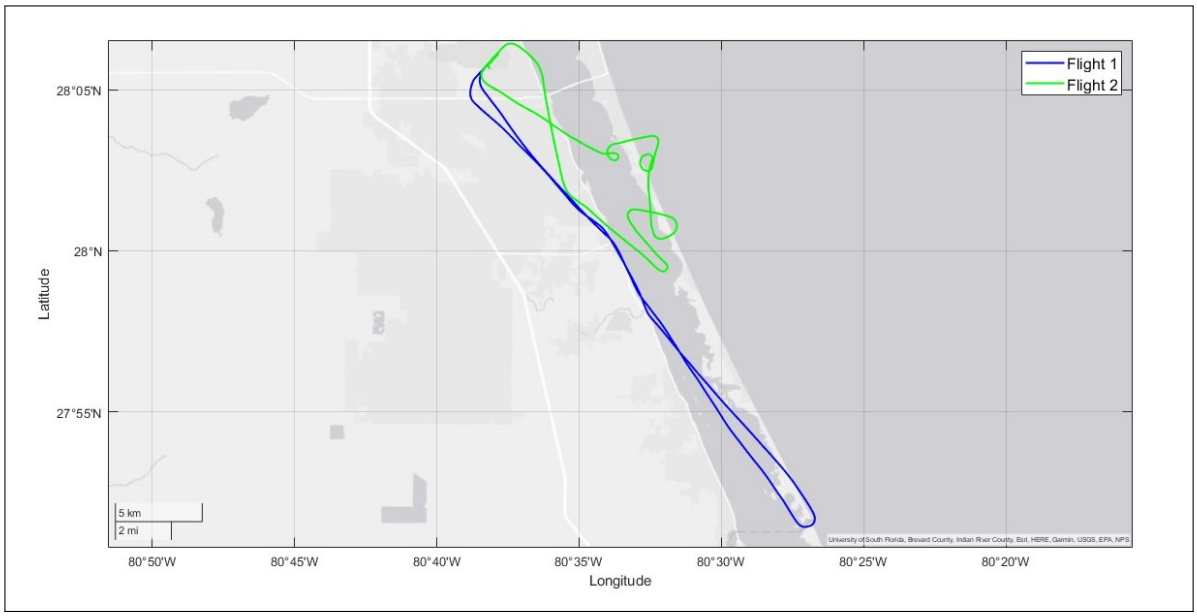

Figure 4.1: N880HM Specific Flight Paths.

Time series charts of indicated airspeed and pressure altitude are depicted in Figure 4.2. The pilot followed the prescribed test profiles accordingly, without any violation of the flight envelope. These data will be analyzed in later sections to evaluate the aircraft's performance under different flight phases.

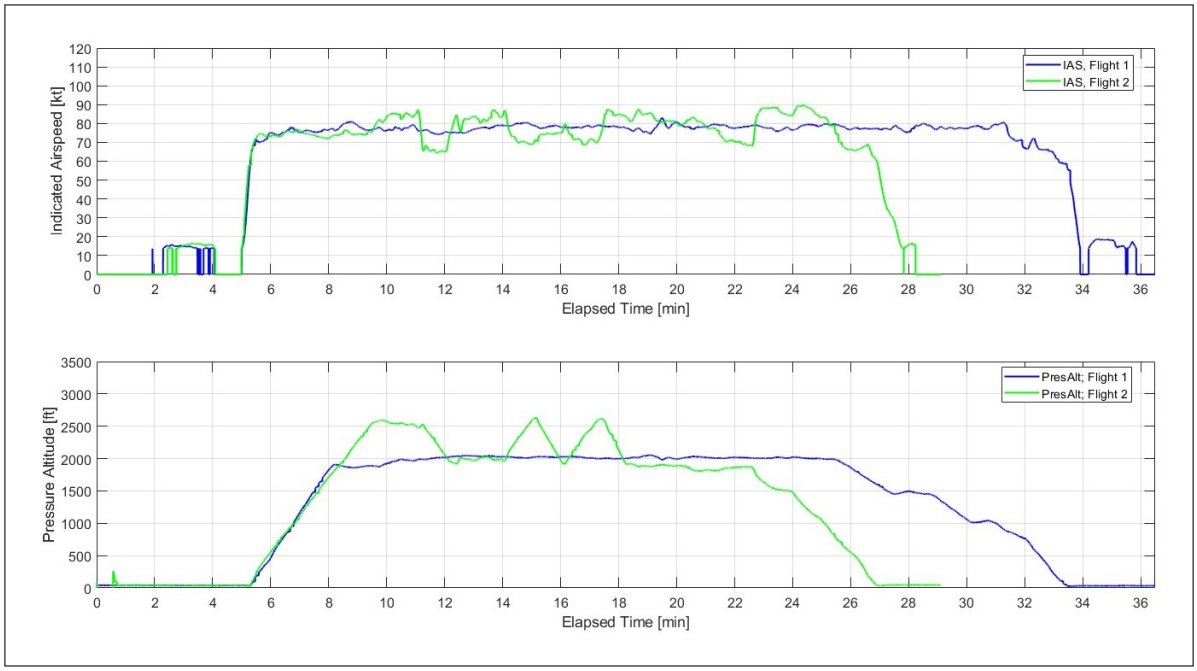

Figure 4.2: Airspeed and Pressure Altitude vs. Elapsed Time.

4.1 Motor Power, RPM, and Torque

The motor power and RPM over the course of each flight are shown in Figure 4.3. Both take-offs were performed with maximum power setting, where a maximum motor power output of nearly 70 kW was achieved.

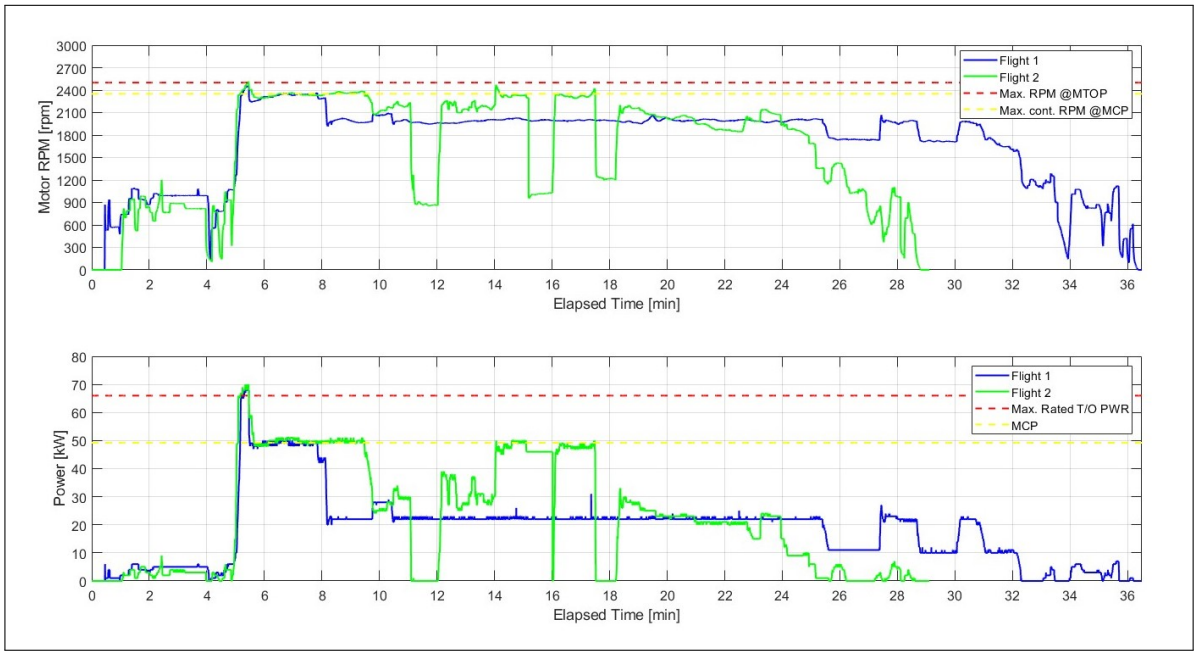

Figure 4.3: Motor Power and RPM vs. Elapsed Time.

As discussed in Section 2, the battery SOC has significant ranges of non-linear behavior on the high and low end of its operation. However, unpredictability in power generation was experienced neither during the take-offs nor along the testings; due to the nature of the flight profiles (Figure 4.4). Therefore, the batteries' ability to supply power was consistent throughout the discharge.

Figure 4.5 depicts motor RPM versus motor power, where a power law relationship pattern is observed. Since the Velis is electronically limited to 2500 rpm, even when there is still power available from the batteries, the RPM cap limits the amount of power that can be delivered to the motor. As no high speed test points close to the V_h were performed, this effect is not evident in the graph.

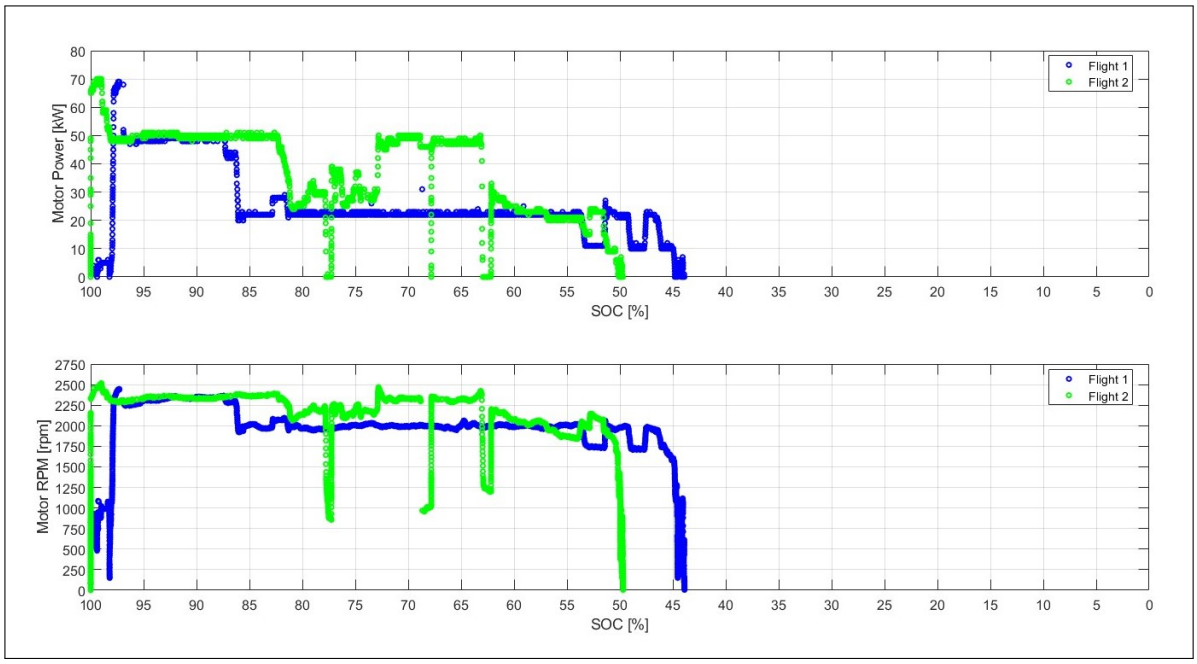

Figure 4.4: Motor Power and RPM vs. SOC.

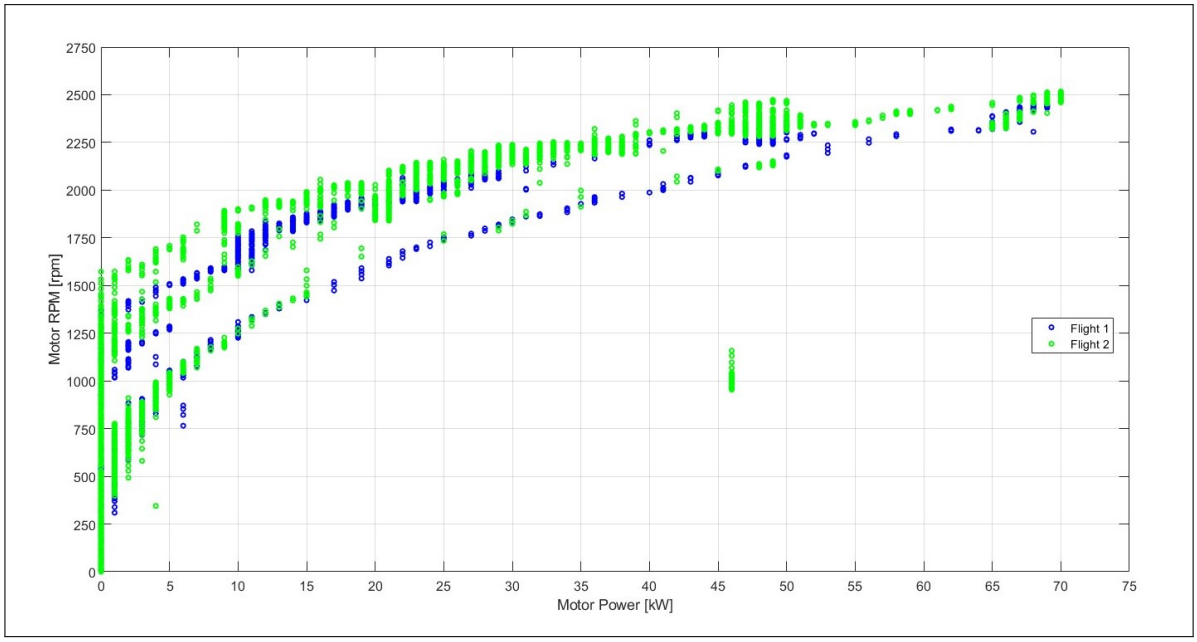

Figure 4.5: Motor RPM vs. Motor Power.

Through motor power and motor RPM, torque output was defined using equation 3.3. The values were normalized and compared with the requested torque extracted from the data logger, as shown in Figure 4.6. Similar to all mechanical systems, electrical

motors experience a reduction in torque when electrical energy is converted to mechanical energy. Consequently, as anticipated, the results illustrated in the figure were clustered above the red diagonal line, implying that the torque requested by the motor controller was greater than the torque output produced by the motor.

A comparable association can be done between the motor power and the power provided by the battery packs (Figure 4.6), which was computed using equation 3.4. After eliminating the outliers, a mean value of approximately 3% in loss of power was found.

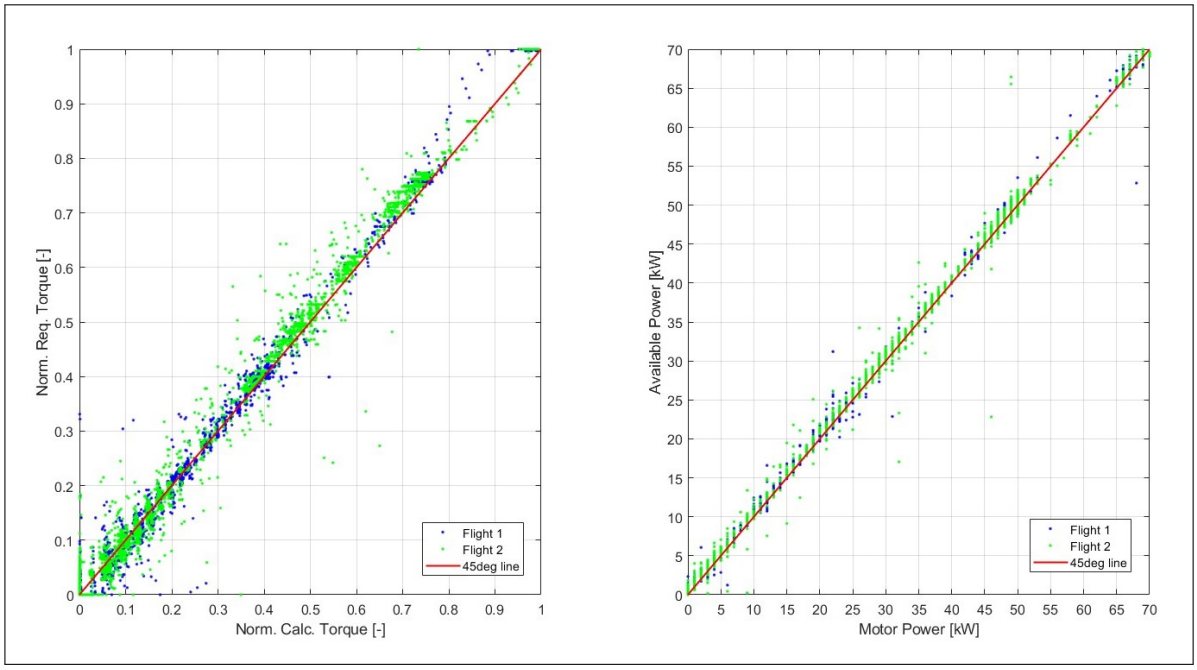

Figure 4.6: a) Normalized Requested Torque vs. Normalized Calculated Torque, b) Power Available vs. Motor Power.

4.2 Powertain System Temperature

The battery cells and motor temperatures were monitored until the end of the test flights. The findings depicted in Figure 4.7 indicate that the thermal management system functioned effectively, ensuring that the components remained significantly below their specified temperature thresholds.

As Flight 1 was conducted on a colder day, the temperatures of the components remained lower than those recorded during Flight 2. Furthermore, even with significant variations in power setting on Flight 2, motor temperatures did not exceed 60°C.

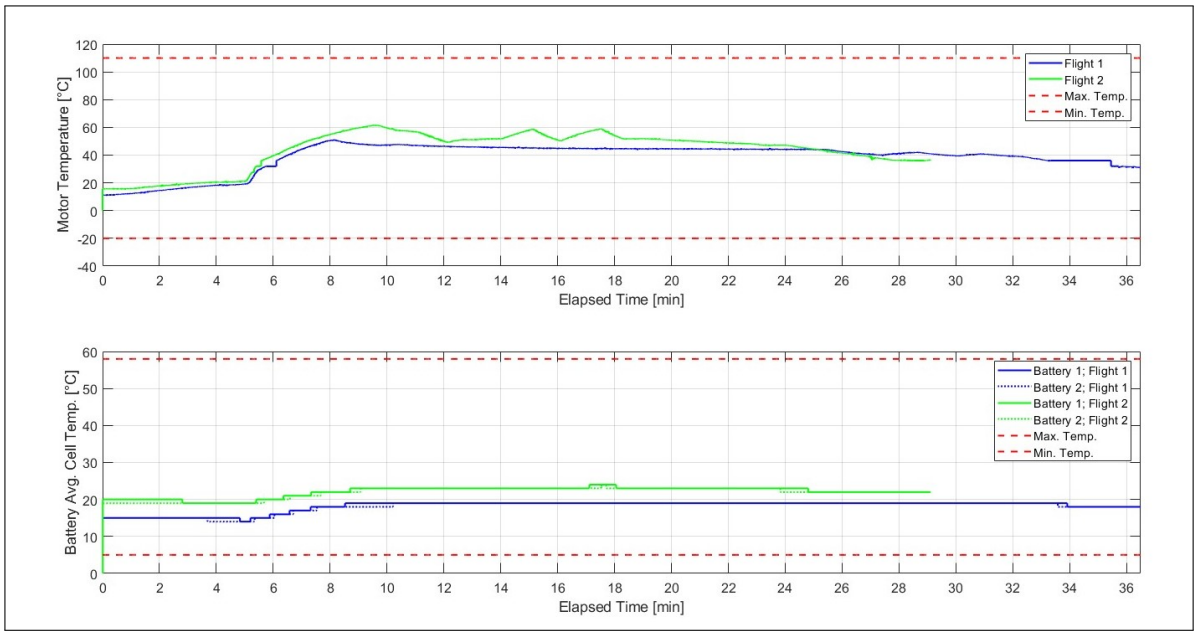

Figure 4.7: Motor and Battery Cells Average Temperatures.

4.3 Battery Performance

Figure 4.8 shows the batteries' voltage and electric current readings obtained during the flights, at a pack level. The data for battery packs 1 and 2 are superimposed on each other, indicating their comparable performance. Additionally, the voltage of the batteries drops as they discharge, which means that the motor controller needs to draw a higher current (refer to equation 3.4) in order to supply power to the motor. This behavior is evident in Flight 1, where a slightly positive slope in discharge current can be observed on cruise flight. Additionally, in the first few minutes of testing, Flight 1 exhibits a slightly lower voltage compared to Flight 2, resulting in a 1% difference. This variation can be attributed to the lower temperature of the battery cells, which reduces their discharge capacity, as discussed in Section 2.

Figure 4.9 presents a time series chart of RFT and SOC, plotted on the same scale. As expected, the curves decrease over time as the motor requires energy. In Flight 2, SOC remains quite non-linear along the discharge due to the variations in the power setting. On the other hand, the SOC in Flight 1 maintains a relatively linear reduction during discharge while on cruise flight. Section 4.4 provides a detailed examination of energy consumption at each flight segment.

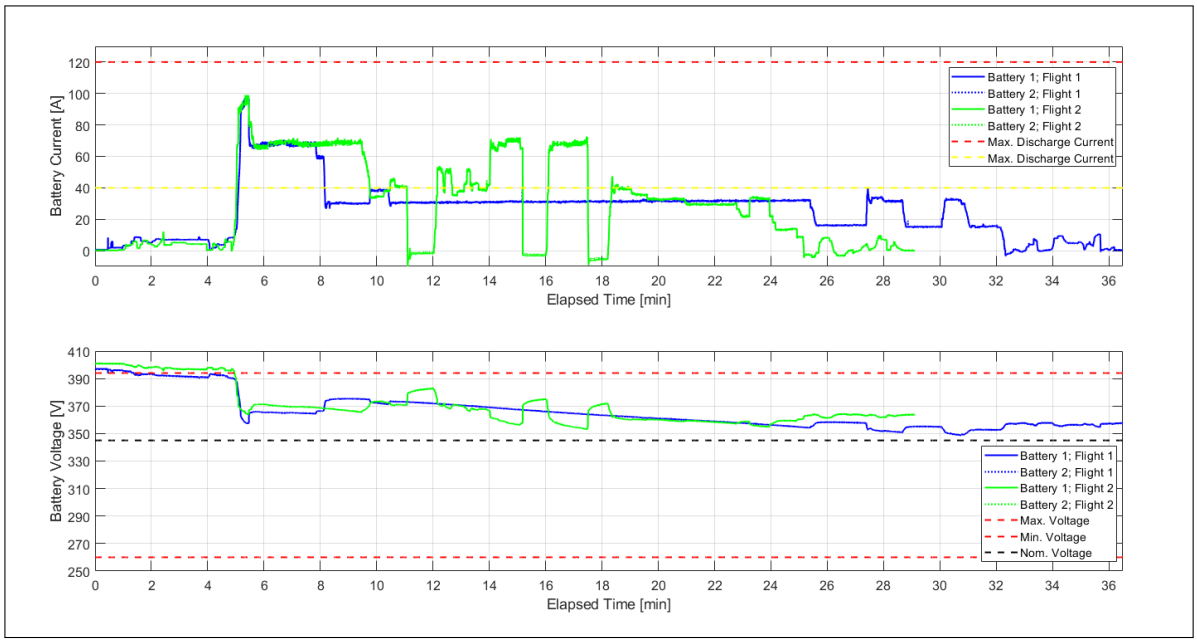

Figure 4.8: Current and Voltage Provided by the Battery Packs vs. Elapsed Time.

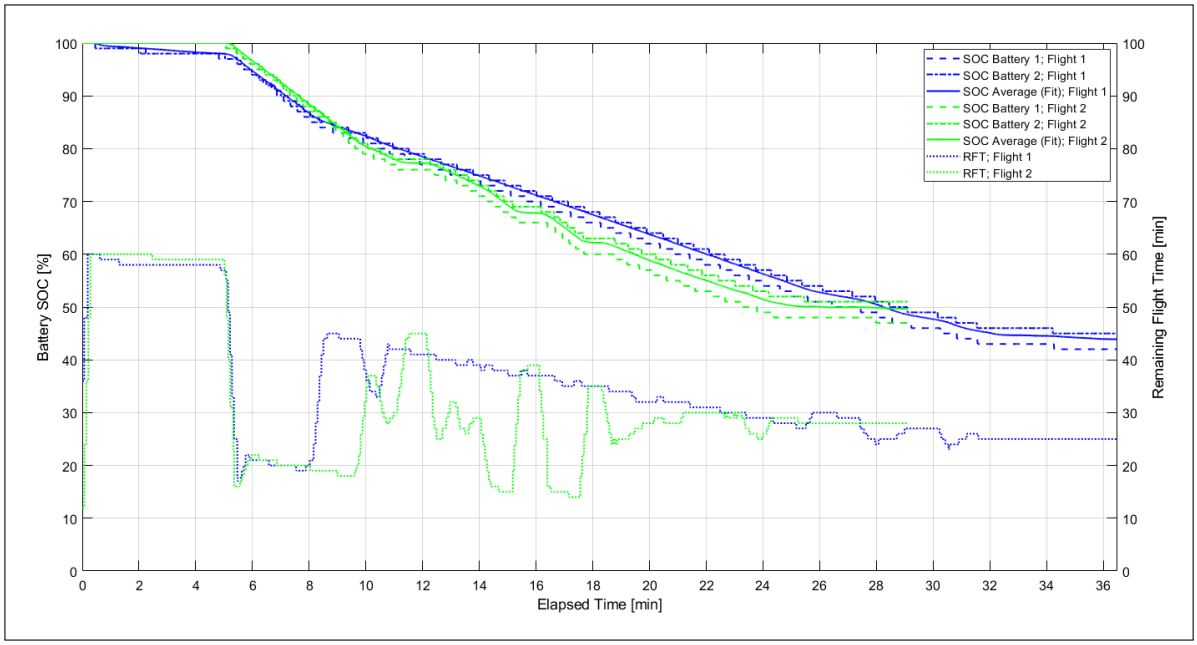

Figure 4.9: SOC and RFT vs. Elapsed Time.

During the discharge process, there appears to be a growing discrepancy between the SOC of batteries 1 and 2. This trend is a result of the differing SOH of the batteries, 7% in Flight 1 and 11% in Flight 2 (Table 4.1), with the effect becoming more pronounced in the battery pack 1. By the end of the test sorties, the difference in SOC between

the batteries was 3% in Flight 1, and 4% in Flight 2. Despite both batteries being installed together in the aircraft by the manufacturer, the contrast in their SOH values is becoming increasingly evident as they cycle. Nevertheless, as observed in Figure 4.8, this difference in SOC was not noticeable, as low values ($< 20\%$) were not reached. The graph also reveals that in both flights the BMS had significantly underestimated the RFT in the first few minutes. In Flight 2, the RFT experienced dips during the MTOP and MCP power settings. Moreover, there were several disagreements between SOC and RFT, potentially creating a confusing decision-making environment for operators.

Finally, as discussed in Section 2, battery internal resistance depends on the battery temperature, age, and SOC. This parameter was calculated using Ohm's Law (equation 3.5) and averaged between both battery packs. The result is graphically presented in Figure 4.10. Data from both flights indicates that internal resistance decreases when battery temperature increases.

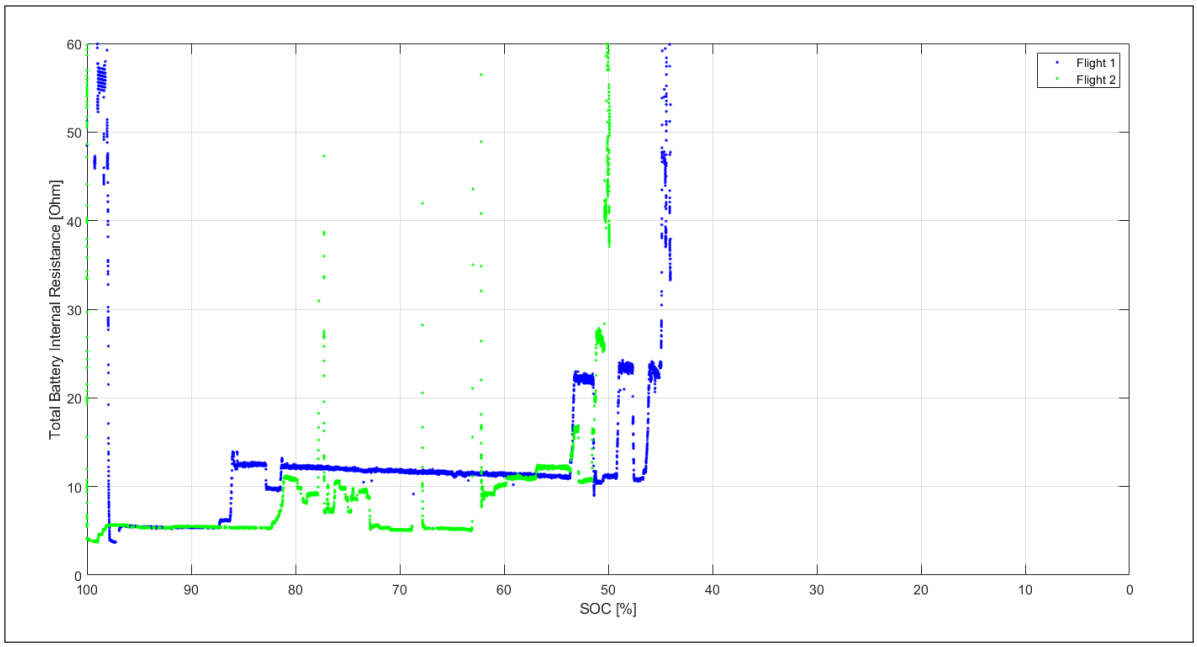

Figure 4.10: Total Battery Internal Resistance vs. SOC.

4.4 Available Energy Required

The available energy indicates the amount of energy that the battery manages to supply the motor controller at a given power setting, considering all losses. Thereby, the available energy reflects real battery performance. In Figure 4.11, the parameter is shown for each battery pack individually, as well as for the sum of both packs. Due to the difference in SOH introduced in Section 4.3, battery pack 2 stores more energy

than pack 1, explaining the shift between the curves.

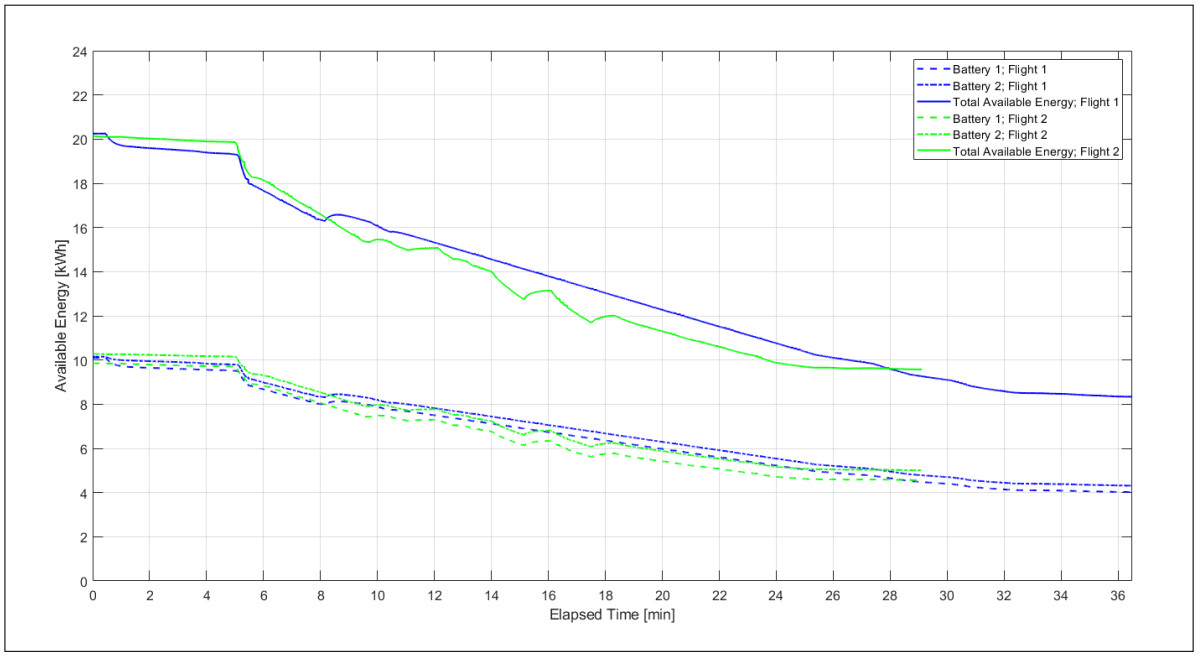

Figure 4.11: Available Energy vs. Elapsed Time.

Tables 4.3 and 4.5 summarize the available energy for each flight segment, where t_i and t_f refer to the starting and ending times of the flight segment. Additionally, the tables state the amount of kWh required at a specific segment over the total kWh required for the entire flight. At engine start, Flight 2 exhibits 2.05% more available energy stored in the batteries than Flight 1, given that both test sorties started with 100% SOC. This characteristic can be attributed to the impact of battery cell temperature, as detailed in Section 2, with Flight 2 exhibiting an average temperature 5°C higher than Flight 1.

It was observed an insignificant correlation between pressure altitude and ROC during climb. In comparison to reciprocating engine aircraft, which lose power at higher altitudes due to the decrease in oxygen availability, the Velis Electro has an outstanding advantage. Since its electric motor does not rely on oxygen for combustion, the aircraft does not experience any power loss as it climbs to higher altitudes. During both flights, the climbs were executed using the maximum continuous power setting (49.2 kW) at an estimated airspeed of 75 kts and 74 kts, respectively. By applying equation 3.9, it was determined that the ROC for Flight 1 was 659 ft/min, while Flight 2 had a lower ROC of 586 ft/min due to the heavier weight of the aircraft. To climb to the same altitude of 1900 ft MSL, Flight 2 required approximately 18% more energy than Flight 1.

Table 4.3: Flight 1: Energy Required For Each Flight Segment.

Mission Segment	Avail. Energy [kWh]	Avail. Energy Required [kWh]
Taxi (t_i) Taxi (t_f)	19.598 19.386	0.212 (1.88%)
Take-off (t_i) Climb (t_f)	19.304 16.318	2.986 (26.51%)
Cruise (t_i) Cruise (t_f)	16.318 10.250	6.068 (53.88%)
Descent (t_i) Landing (t_f)	10.250 8.488	1.762 (15.64%)
Taxi (t_i) Taxi (t_f)	8.488 8.337	0.151 (1.34%)
Total	-	11.261 (100%)

Table 4.5: Flight 2: Energy Required For Each Flight Segment.

Mission Segment	Avail. Energy [kWh]	Avail. Energy Required [kWh]
Taxi (t_i) Taxi (t_f)	19.999 19.894	0.105 (1.00%)
Take-off (t_i) Climb (t_f)	19.860 16.338	3.522 (33.78%)
Training Maneuvers (t_i) Training Maneuvers (t_f)	16.318 10.250	5.953 (57.10%)
Descent (t_i) Landing (t_f)	10.385 9.628	0.757 (7.26%)
Taxi (t_i) Taxi (t_f)	9.628 9.574	0.054 (0.51%)
Total	-	10.425 (100%)

During Flight 1, the pilot maintained a power setting of 22 kW while in cruise flight, resulting in an average airspeed of 78 kts and a covered distance of 22.87 NM. As observed in Table 4.5, this flight regime required 53.88% of the total available energy required to complete the test sortie. Figure 4.12 demonstrates that a steady, linear

increase in the distance traveled was attained. Via equations 3.6 and 3.7, it was calculated a SR of 3.5 NM/kWh and a SE of 2.6 min/kWh.

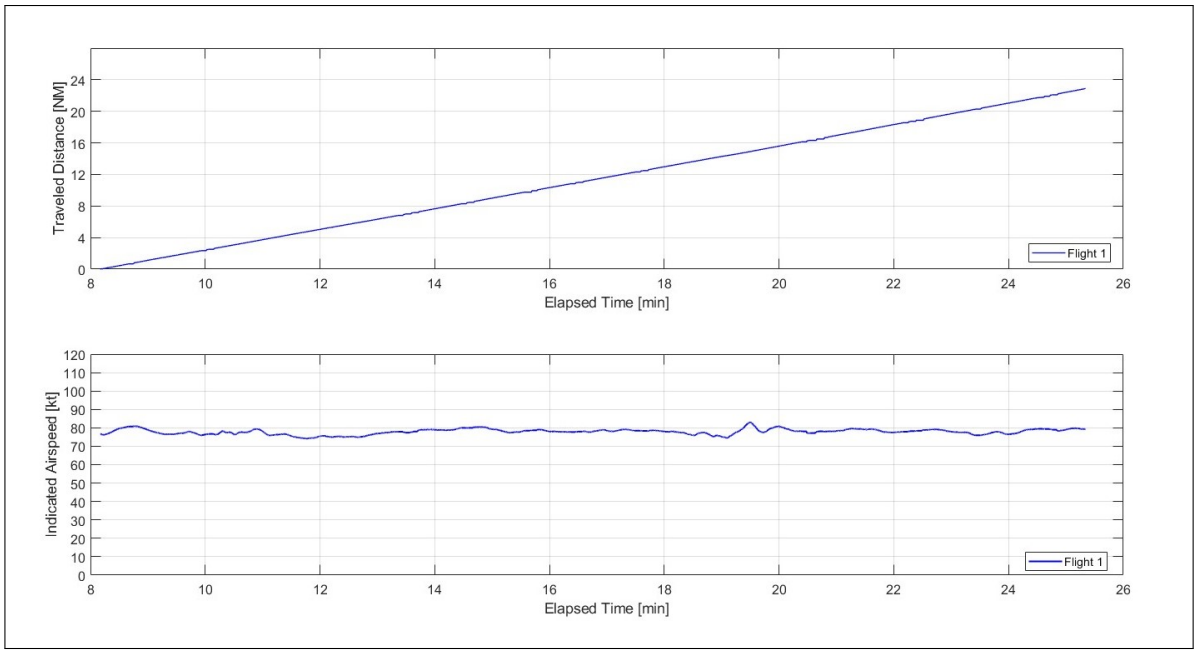

Figure 4.12: Flight 1: Traveled Distance and Airspeed During Cruise Flight.

In Flight 2, the pilot trimmed the aircraft with 21 kW at nearly 2000 ft, stabilizing at 69 kts. Under this condition, the estimated SR was 3.9 NM/kWh and the SE was 2.9 min/kWh. Despite flying at a lower airspeed and with a heavier weight, it is worth noting that this value of SR is 12.85% higher than that calculated for Flight 1. This counterintuitive outcome is attributed to the difference in OAT and reinforces the importance of understanding the impacts of temperature on battery performance while planning the flight.

In addition, sustained turns with 30° of bank angle were performed with a target airspeed of 85 kts. To execute the maneuver, approximately 0.52 kWh was required. This represents a 17% increase in energy required compared to the amount required to trim the aircraft at a steady flight with the same airspeed.

An initial descent in Flight 1 lasted 6 minutes, at which point the aircraft maintained a cruise airspeed of 78 kts and descended at a rate of descent of approximately -172 ft/min, covering a distance of 7.7 NM. This phase of the flight required 1.52 kWh of energy. Subsequently, during the approach for landing, the aircraft descended at a rate of descent of approximately -422 ft/min. Whereas in Flight 2, the descent was performed with a rate of descent of -485 ft/min. As a result, Flight 1 required a significantly greater amount of available energy than Flight 2 at this flight segment. Furthermore,

the taxi from the hangar to the runway in Flight 1 consumed more energy due to the different runway used for takeoff and landing.

Chapter 5

Conclusion

This work examined the battery performance of the Pipistrel Velis Electro under two different prescribed flight profiles and take-off weights; both started with a fully charged battery (100% SOC) and were completed before SOC dropped below 40%, to ensure 30 minutes of energy reserve. The profiles were based on the GAMA Publication 16, which is frequently used as a baseline in hybrid and electric aircraft research. Flight 1, which is the destination trip profile, was performed with a gross weight of 1146 lbs and with a constant power setting of 22 kW during the cruise flight. On the other hand, Flight 2 represented a local training flight profile, where maneuvers such as simulated power-off descents and sustained level turns were performed with a gross weight of 1318 lbs. Consequently, it exhibited more pronounced variations in power setting in comparison to Flight 1. OAT varied from 11°C in Flight 1 to 15°C in Flight 2.

The analysis of motor power shows that the unpredictability in power generation was not experienced during testing, and the batteries' ability to supply power was consistent throughout the discharge. The mean value of approximately 3% in power loss was found during the conversion of power provided by the battery packs to motor power. This demonstrates the high efficiency of the axial flux AC motor and its potential as a convenient option for electric aircraft.

The superimposition of the voltage and electrical current data for battery packs 1 and 2 indicates their comparable performance. However, a growing discrepancy between the SOC of the batteries was observed during the discharge process due to the difference in SOH, resulting in one battery storing more energy than the other. In Flight 2, the SOC is non-linear during discharge due to power setting variations, while in Flight 1, SOC drops quite linearly during cruise flight. The BMS initially underestimated flight time during testing, which could have made decision-making challenging for the operators.

The energy required analysis shows that Flight 2 had 2.05% more available energy

at engine start than Flight 1 due to the difference in the OAT during battery charging. To climb to the same altitude of 1900 ft MSL, Flight 2 required approximately 18% more energy than Flight 1. In the cruise segment, Flight 1 exhibited a specific range of 3.5 NM/kWh and specific endurance of 2.6 min/kWh using 22 kW, while Flight 2 achieved 3.9 NM/kWh and 2.9 min/kWh with 21 kW, despite the higher weight. This counterintuitive outcome is attributed to the difference in OAT and reinforces the importance of understanding the impacts of temperature on battery performance while planning the flight. Additionally, sustained turns with 30° of bank angle were performed at a target airspeed of 85 kts, requiring approximately 0.52 kWh to complete the maneuver. This represents a 17% increase in energy required compared to the amount required to trim the aircraft at a steady flight with the same airspeed.

The high aspect ratio of the Velis makes it more sensitive to external factors such as airmass, air quality, and the pilot's handling techniques. The pilot reported that significant differences in energy required were observed during maneuvers and flight conditions replicated in different sorties, highlighting the importance of consistent testing methods and data analysis. These findings underscore the importance of considering maneuvering energy required when establishing safety margins for electric aircraft operations. This point deserves the attention of regulatory authorities, who play a critical role in ensuring safe and efficient operations. Moreover, future testing is recommended to assess the impact of longitudinal and lateral acceleration resulting from the external factors on TEM.

Bibliography

[1] A. Farmann and D. U. Sauer. "A comprehensive review of on-board State-of-Available-Power prediction techniques for lithium-ion batteries in electric vehicles". *Journal of Power Sources*, 2016. no. 329, pp. 123-137.

[2] Aviation Week. FAA Releases First eVTOL Certification Basis For Comment, 2022. Last accessed January 27, 2023, `https://aviationweek.com/air-transport/faa-releases-first-evtol-certification-basis-comment#:~:text=But%20in%20May%20this%20year,under%20Part%2021.17(b).`

[3] European Union. "Easy Access Rules for Air Operations (Regulation (EU) No 965/2012), ED Decision 2022/005/R, AMC1 NCO.OP.125. Page 1837", 2022. Last accessed February 05, 2023, `https://www.easa.europa.eu/downloads/20342/en`.

[4] FAA. "Small Airplane Issues List (SAIL), Q2 FY 2019 Release", 2019. Last accessed February 16, 2023, `https://www.faa.gov/aircraft/air_cert/design_approvals/small_airplanes/small_airplanes_regs/media/sail_fy19_q2.pdf`.

[5] Favier, A., Roberts, S., Esfeld, J., and Uchida, J. "Things Flight Testers Should Know About Batteries for Electric Propulsion". *52nd SFTE International Symposium*, 2021. St. Louis, MO, 2021.

[6] GAMA. "GAMA Publication No. 16: Hybrid & Electric Propulsion Performance Measurement". *General Aviation Manufacturers Association*, 2017. Washington, DC.

[7] Kim, D., Verberne, J., Sotiropoulos-Georgiopoulos, E., Harrison, E., and Mavris, D. "A Model-Based System Engineering Approach to the Certification of Transport Type Aircraft". *AIAA SciTech 2022 Forum*, 2021. San Diego, California. (Published). Retrieved February 17, 2023, from `https://doi.org/10.2514/6.2022-2550`.

[8] Kimberlin, Ralph. D. *Flight Testing of Fixed-Wing Aircraft*. AIAA, 2003.

[9] Lance W. Traub. Range and Endurance Estimates for Battery-Powered Aircraft. *JOURNAL OF AIRCRAFT, Vol. 48, No. 2*, 2011. Engineering Notes. Embry-Riddle Aeronautical University, Prescott, Arizona 86301.

[10] M. R. Palacin, and A. de Guibert. "Why do batteries fail?". *Science*, 2016. vol. 351, no. 6273.

[11] Mohamad Aris, Asma & Shabani, Bahman. "An Experimental Study of a Lithium Ion Cell Operation at Low Temperature Conditions". *Energy Procedia*, 2017. 110. 128-135.10.1016/j.egypro.2017.03.117.

[12] Notten, Peter & Veld, Bert & Beek, J.R.G. "Boostcharging Li-ion batteries: A challenging new charging concept". *Journal of Power Sources*, 2005. 145. 89-94.10.1016/j.jpowsour.2004.12.038.

[13] Pipistrel Vertical Solutions d.o.o. PILOT'S OPERATING HANDBOOK, VELIS Electro Non Type Certified. Vipavska cesta 2, SI-5270 Ajdovščina, Slovenia, revision: a00 edition (May). Document No.: POH-X128-00-40-001., 2021b.

[14] Rozas, H., Troncoso-Kurtovic, D., Ley, C. P., and Orchard, M. E. Lithium-ion battery State-of-Latent-Energy (SoLE): A fresh new look to the problem of energy autonomy prognostics in storage systems. *Journal of Energy Storage*, 2021. 40(2021), 102735, Retrieved March 12, 2023, from `https://doi.org/10.1016/j.est.2021.102735`.

[15] The Driven. Electric planes are coming: Short-hop flights could be running on batteries in a few years, 2022. Last accessed January 24, 2023, `https://rb.gy/rw5zlt`.

[16] Tom, L., Khowja, M., Vakil, G., and Gerada, C. "Commercial Aircraft Electrification—Current State and Future Scope". *Energies*, 2021. Retrieved January 26, 2023, from `https://doi.org/10.3390/en14248381`.

[17] Verberne, J., Beedie, S., Harris, C., Justin, C., and Mavris, D. "Development of a Simulation Environment to Track Key Metrics to Support Trajectory Energy Management of Electric Aircraft". *AIAA Aviation 2022 Forum*, 2022. Chicago, Illinois. (Published). Retrieved February 17, 2023, from `https://doi.org/10.2514/6.2022-3255`.

[18] Wilde, M., Kish, B., Senkans, E., Kanchwala, T., Beedie, S., Harris, C., Verberne, J., Justin, C., and Merkt, J. "Trajectory Energy Management Systems for eVTOL Vehicles: Modeling, Simulation and Testing". *AIAA Aviation Forum*, 2022. Virtual. (Published). Retrieved February 17, 2023, from `https://doi.org/10.2514/6.2022-3413`.

[19] Xu, Z., Wang , J., Fan, Q., Lund, P. D., and Hong, J. "Improving the state of charge estimation of reused lithium-ion batteries by abating hysteresis using machine learning technique". *Journal of Energy Storage*, 2020. vol. 32, 2020, 101678, ISSN 2352-152X. Retrieved February 20, 2023, from `https://doi.org/10.1016/j.est.2020.101678`.